applied sciences

MDPI

Article

Design and Performance Evaluation of an In Situ Online Soil Electrical Conductivity Sensor Prototype Based on the High-Performance Integrated Chip AD5941

Runze Song [1] and Man Zhang [2,*]

[1] Key Laboratory of Smart Agriculture System Integration, China Agricultural University, Ministry of Education, Beijing 100083, China; rzsong@cau.edu.cn
[2] Key Laboratory of Agricultural Information Acquisition Technology, China Agricultural University, Ministry of Agriculture and Rural Affairs, Beijing 100083, China
* Correspondence: cauzm@cau.edu.cn

Abstract: Soil electrical conductivity has an important influence on the growth and development of plants. The existing real-time soil electrical conductivity detection device is affected by temperature, inconvenient to use, expensive, etc.; therefore, based on the classical four-terminal method of soil electrical conductivity detection principle, in this study, we aim to improve the limitations of the constant current source, selecting the high-performance integrated chip AD5941, optimizing the detection circuit and probe structure, improving the achievability of the detection circuit, and designing a type of in situ on-line real-time access to a soil electrical conductivity detection device, and improve the detection accuracy by temperature compensation. In this paper, dynamic performance, steady state performance, radial sensitivity range, and calibration test are carried out for the soil electrical conductivity detection prototype. The test results show that the dynamic response speed of the prototype is less than 50 ms, the steady state error is not more than ±2%, and the radial measurement sensitivity range is 8~10 cm. A comparison with the commercial sensor shows that the linear fit of the two measurements reaches 0.9995, and the absolute error ranges from −61.40 μS/cm to 23.90 μS/cm, with a relative error range of −1.94~1.86%. It shows that the performance of the two sensors is comparable, but the quality/price ratio of the prototype is much higher than that of the commercialized product. In this study, it is demonstrated that a high-precision, low-cost, and easy-to-use in situ online soil electrical conductivity detection device can be provided for agricultural and forestry production.

Keywords: soil electrical conductivity; in situ measurement; AD5941; temperature compensation

Citation: Song, R.; Zhang, M. Design and Performance Evaluation of an In Situ Online Soil Electrical Conductivity Sensor Prototype Based on the High-Performance Integrated Chip AD5941. *Appl. Sci.* **2024**, *14*, 7788. https://doi.org/10.3390/app14177788

Academic Editors: Paweł Kiełbasa, Anna Miernik and Akinniyi Akinsunmade

Received: 22 July 2024
Revised: 25 August 2024
Accepted: 27 August 2024
Published: 3 September 2024

1. Introduction

Soil electrical conductivity is a crucial parameter that reflects soil conditions, significantly affecting crop health and yield [1,2] and influencing several critical plant growth parameters [3–6]. The rapid acquisition of soil electrical conductivity data provides effective support for precise agricultural management, offering valuable guidance for optimizing agricultural practices.

The research on real-time soil electrical conductivity acquisition methods by scholars both domestically and internationally dates back to the 20th century [7], with sustained high interest in this field. The primary methods include soil solution conductivity measurement, soil electrical conductivity measurement based on electromagnetic induction (EM) technology [8,9], soil electrical conductivity measurement based on spectroscopy [10,11], and soil electrical conductivity measurement using the four-terminal method [12]. Among these, the soil solution conductivity measurement offers high accuracy but requires a prolonged detection time, making it unsuitable for monitoring in arid regions. The four-terminal

method for soil electrical conductivity measurement is currently the most widely used technology, having been thoroughly validated, widely promoted, and extensively applied.

With the advances in research into the "four-terminal method" for soil electrical conductivity detection, improving measurement accuracy, reducing production costs, enhancing practicality, and minimizing equipment power consumption have become shared goals among scholars and manufacturers globally. The "four-terminal method" has evolved from its initial DC principle to the widely adopted AC principle, addressing issues such as sensor electrolysis when buried in soil for extended periods, which previously compromised detection accuracy and sensor longevity. Currently, the principles of the "four-terminal method" for soil electrical conductivity detection are well-established. Researchers now focus on optimizing the sensor structural design, detection circuit implementation, and mitigating influencing factors to enhance detection accuracy and practicality across various application scenarios. For instance, Xiaoshuai Pei et al. [13] expanded the standard four-pin structure to a six-pin configuration, enabling the simultaneous detection of soil electrical conductivity (EC) at two different depths. In this design, the two central pins measure the shallow soil layer EC, the two outer pins measure the deep soil layer EC, and the two middle pins provide the driving current. Xiangjun Zhong et al. [14] utilized an STM32 processor as the core, integrating power supply circuits, AC signal source circuits, RMS detection circuits, and other peripheral circuits to develop a discrete component AC "four-terminal method" soil electrical conductivity detection circuit. Wei Yang et al. [15] applied the "four-terminal method" to field vehicle-mounted soil detection, using a signal generator instead of a constant current source to provide larger amplitude and more stable sinusoidal signals, thereby advancing a soil electrical conductivity detection system based on a digital oscilloscope. Cristina Rusu et al. [16] introduced a miniature, low-power, real-time, multi-parameter, and cost-effective soil electrical conductivity sensor.

Previous studies have utilized the "four-terminal method" to investigate soil electrical conductivity acquisition, resulting in the development of several products [17,18]. Despite these advances, the following three critical issues remain insufficiently addressed:

(1) The detection principle relies on a constant current source, necessitating the use of discrete components to construct the detection circuit. This approach results in low integration, which not only impedes further improvements in detection accuracy but also leads to high power consumption and increased costs.
(2) Previous studies have predominantly used needle-type probe structures, which are inconvenient to use with hard soil and are prone to sensor damage.
(3) Numerous studies have shown that the soil electrical conductivity is affected by temperature, and electronic products also suffer from temperature drift issues. Currently, the "four-terminal method" soil electrical conductivity detection products lack effective research on temperature compensation methods.

This paper addresses the aforementioned issues by improving the principles of the soil electrical conductivity sensor based on the "four-terminal method", optimizing the measurement circuit and structure, and incorporating temperature compensation. These efforts aim to enhance the detection accuracy and usability of the "four-terminal method" soil electrical conductivity sensor, laying the groundwork for the localization of the equipment.

2. Materials and Methods

2.1. Improved In Situ Online Measurement Principle of Soil Electrical Conductivity with Four-Terminal Electrodes

The resistivity method, also referred to as the four-terminal or four-electrode method, employs sensors designed with four electrodes or probes typically arranged in a linear configuration. In this setup, the outer electrodes (F+ and F−) serve as the excitation terminals, while the inner electrodes (S+ and S−) act as the measurement terminals, as illustrated in Figure 1.

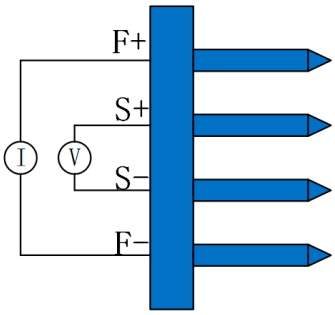

Figure 1. Conventional four-terminal method of soil electrical conductivity detection principle. F+ and F− indicate the outer electrodes for excitation terminals, S+ and S− indicate the inner electrodes for measurement terminals, V indicates the voltage meter, and I indicates the current source.

A constant current I is applied to the excitation terminal in the conventional four-terminal method, and the conductivity *ECa* of the soil is converted by measuring the voltage *V* across *S*+ and *S*−, as shown in Equation (1):

$$EC_a = \frac{1}{V} I \frac{\frac{1}{L_{F+S+}} - \frac{1}{L_{S+S-}} - \frac{1}{L_{F+S-}} + \frac{1}{L_{S-F-}}}{2\pi} \quad (1)$$

where L_{F+S+}, L_{S+S-}, L_{F+S-}, and L_{S-F-} represent the respective distances between the electrodes. V represents the potential difference measured across the electrodes S+ and S−, and I represents the constant current output by the excitation electrodes F+ and F−.

When the four electrodes are arranged in a straight line and equidistant, it can be expressed as $L_{F+S+} = L_{S+S-} = L_{S-F-} = d$. This electrode configuration constitutes the Wenner configuration [14], and the above formula can be simplified to the following:

$$EC_a = \frac{1}{V} I \frac{1}{2\pi d} \quad (2)$$

From the above equation, it is evident that when the current remains constant, the electrical conductivity (EC_a) is inversely proportional to the potential difference across the measuring electrodes S+ and S−. Consequently, this relationship forms the basis for determining soil electrical conductivity using this method.

The conventional "four-terminal method" for detecting soil electrical conductivity necessitates a constant excitation current (I). This method employs a detection circuit comprising discrete, low-integration components, which are susceptible to systematic errors and contribute to increased unreliability due to the interactions among these components. If the excitation current (I) is not constant, Equation (2) changes to the following:

$$EC_a = \frac{1}{\frac{V}{I}} \cdot \frac{1}{2\pi d} = \frac{1}{R} \cdot \frac{1}{2\pi d} \quad (3)$$

where R denotes the probe impedance.

It is evident that the soil electrical conductivity exhibits a linear relationship with the reciprocal of the probe impedance. Consequently, soil electrical conductivity can be determined by measuring the probe impedance. Equation (3) offers a theoretical foundation for the "four-terminal method" of soil electrical conductivity detection using a non-constant current source design.

2.2. Soil Electrical Conductivity Prototype Design

2.2.1. Prototype Cone Probe Structure Design

Traditional multi-pin soil electrical conductivity sensor configurations [19–21] encounter issues related to user inconvenience and susceptibility to damage. To address these challenges and enhance ease of insertion into the soil, this study adheres to the American

Society of Agricultural Engineers (ASAE) standards by designing a cone-type probe [22,23] featuring a 30° cone angle and four ring electrodes. This design aims to improve the sensor's maneuverability and robustness [24].

Figure 2 illustrates the four-electrode ring probe, with electrodes designated as F+, S+, S−, and F− sequentially from top to bottom. In soil electrical conductivity measurements, the F+ and F− electrodes serve as the excitation electrodes, while the S+ and S− electrodes function as the measurement electrodes. The light grey component represents an insulating ring that separates the four electrodes. Additionally, the conical head at the bottom houses an internally encapsulated temperature sensor, which is connected to the acquisition main board via four wires.

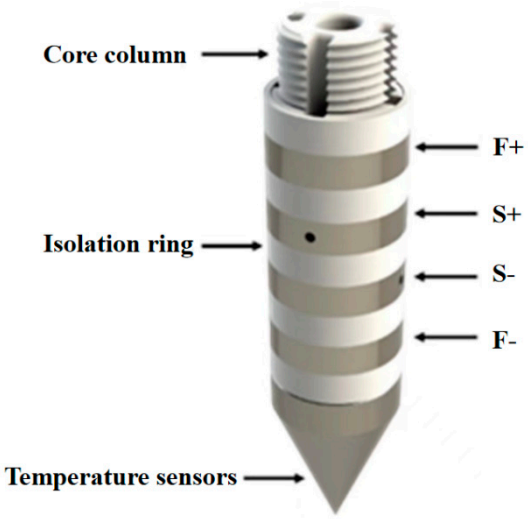

Figure 2. Ring probe structure diagram.

2.2.2. Hardware Design of Soil Electrical Conductivity Prototype

As depicted in Figure 3, the soil electrical conductivity prototype comprises several modules, as follows: a conductivity detection module, a temperature detection module, a main control module, a storage module, a communication module, and a power control module. The core of the main control module is a low−power, high−performance STM32 chip. The main control module interfaces with the detection modules (soil electrical conductivity and temperature), the storage module, the communication module, and the power control module via communication protocols such as I2C, SPI, and UART.

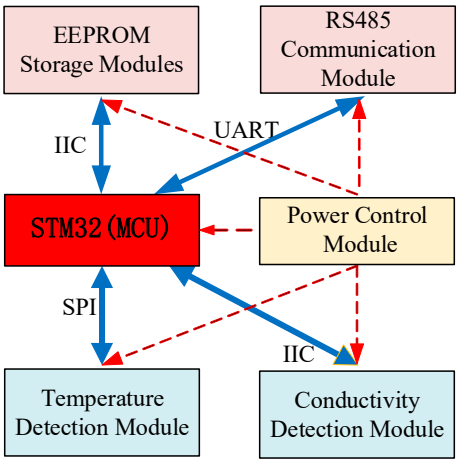

Figure 3. Schematic diagram of prototype hardware system structure.

The primary focus of this paper is the design of the soil electrical conductivity detection module. Traditional four−terminal conductivity measurement systems typically comprise discrete components, including an excitation signal generation circuit, an AC constant−current drive circuit, a range switching circuit, and an RMS detection circuit. This approach results in a sensor with numerous components, leading to high circuit complexity and elevated costs, thereby hindering widespread application and adoption.

In this thesis, the soil electrical conductivity detection module utilizes the low−power analog front−end chip AD5941 from Analog Devices Inc. (ADI, USA), which incorporates a high−precision excitation loop, a programmable switching matrix, a general− purpose ADC channel, and a DFT module, among other features [25]. This chip offers extensive reprogramming capabilities. Leveraging the principles of the improved "four−terminal method" for soil electrical conductivity detection, our team strategically combined the chip's on−board resources to implement absolute impedance measurement, thereby facilitating accurate soil electrical conductivity measurement, as illustrated in Figure 4.

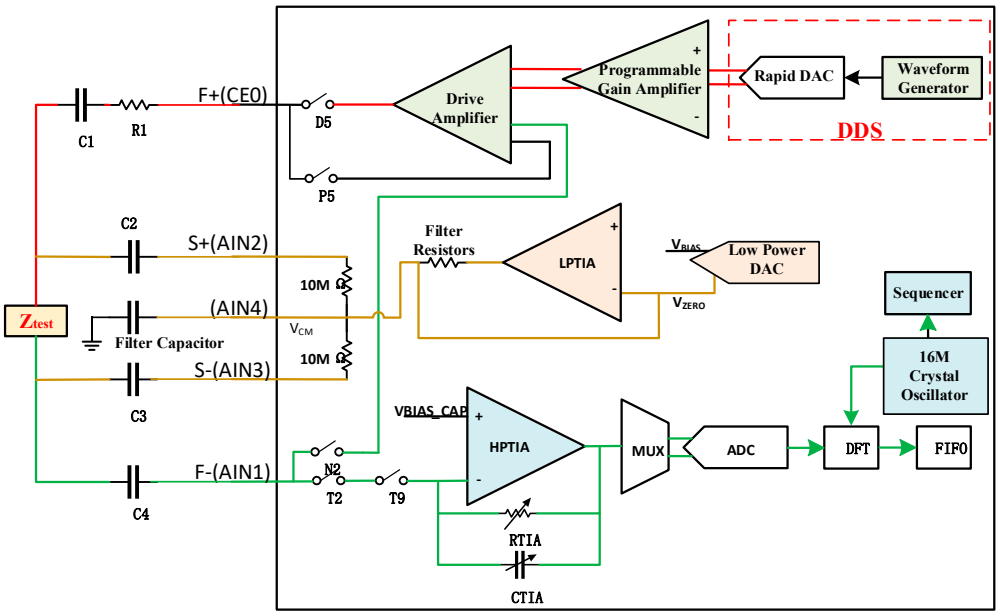

Figure 4. Schematic diagram of soil electrical conductivity measurement principle.

The working process is as follows:

(1) The waveform generator within the AD5941, in conjunction with the high−speed DAC, is configured to form a digital frequency synthesizer (DDS), capable of producing a 100 kHz sine wave excitation signal with a 30−bit resolution;
(2) The sine wave excitation signal is routed through a programmable gain amplifier (PGA) and an excitation amplifier, emerging from the F+ (CE0) port. Subsequently, it passes through the isolation capacitor C1, forming an AC signal (I) that is applied to the impedance to be measured (soil probe, Ztest);
(3) The AC signal (I) then flows through F− (AIN1) and is converted into a voltage signal via a high−performance transimpedance amplifier (HPTIA). This signal is biased to 1.11 V to ensure compatibility with the ADC's input range;
(4) After the ADC samples this voltage signal, the data are processed by the DFT module, yielding the real and imaginary components of the current frequency;
(5) Subsequently, the ADC's input source is switched to the voltage measurement paths S+ (AIN2) and S− (AIN3) by closing N2 and disconnecting T2 via the multiplexer (MUX);
(6) The voltage (V) at the current frequency is then measured, sampled by the ADC, and processed by the DFT module to obtain the corresponding real and imaginary voltage components;

(7) From these real and imaginary components of the voltage (V) and current (I), the respective amplitude and phase are calculated and stored in the FIFO register.

The microcontroller unit (MCU) retrieves the real and imaginary components of the voltage and current from the FIFO registers, converts these components into amplitude and phase, and then applies the following formula to determine the magnitude and phase of the measured impedance, as presented in Equation (4).

$$\begin{cases} |Z_{test}| = \frac{Voltage\ Magnitude}{Current\ Magnitude} \times R_{TIA} \\ \theta = Voltage\ Phase - Current\ Phase + C_{TIA} \end{cases} \quad (4)$$

where voltage magnitude is voltage amplitude; current magnitude is current amplitude; RTIA is the programmable resistors within high speed TIA; CTIA is the programmable capacitors within high speed TIA; Ztest is the phase ofimpedance. At this point, the real (resistive) component of the impedance is then calculated. The soil electrical conductivity can be obtained by substituting it into the modified four−terminal method soil electrical conductivity test shown in Equation (3).

The soil electrical conductivity prototype comprises the following three circuit board layers: a detection board, a voltage board, and a main control board, along with a probe, as depicted in Figure 5. The outer housing has a diameter of 50 mm and a height of 75 mm, while the probe itself has a diameter of 16 mm and a height of 76.5 mm.

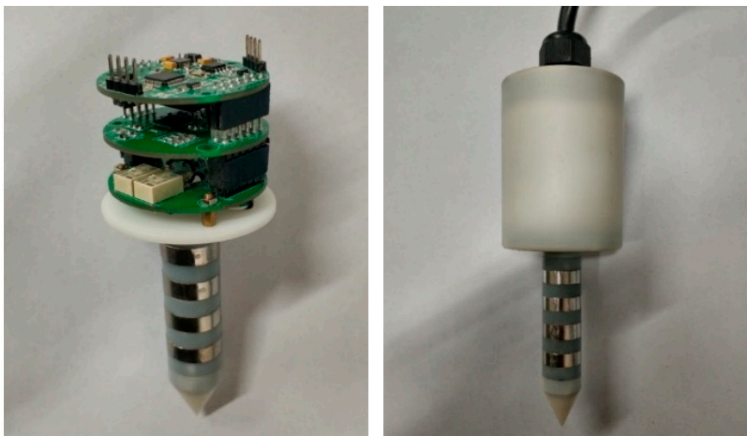

Figure 5. Soil electrical conductivity prototype.

2.2.3. Software Design for Soil Electrical Conductivity Detection

The software for the soil electrical conductivity detection system primarily facilitates system initialization, time−sharing acquisition, and the processing of soil electrical conductivity and temperature data. It also enables the setting of prototype calibration coefficients, temperature compensation coefficients, and the configuration of prototype addresses and serial numbers.

The primary objective of prototype initialization is to configure the MCU's internal resources and to set up the peripherals and pins utilized by each measurement module, as illustrated in Figure 6. The system operates at a frequency of 72 MHz, with the RS485 serial port configured to a baud rate of 9600. The EEPROM module and the TMP117 temperature module are assigned addresses of 0×50 and 0×48, respectively, through pin electrical connections. To ensure reliable operation despite potential electromagnetic interference or other factors that could cause the program to enter an abnormal state, the system employs the STM32's internal independent watchdog, set with a reset time of 1.6 s.

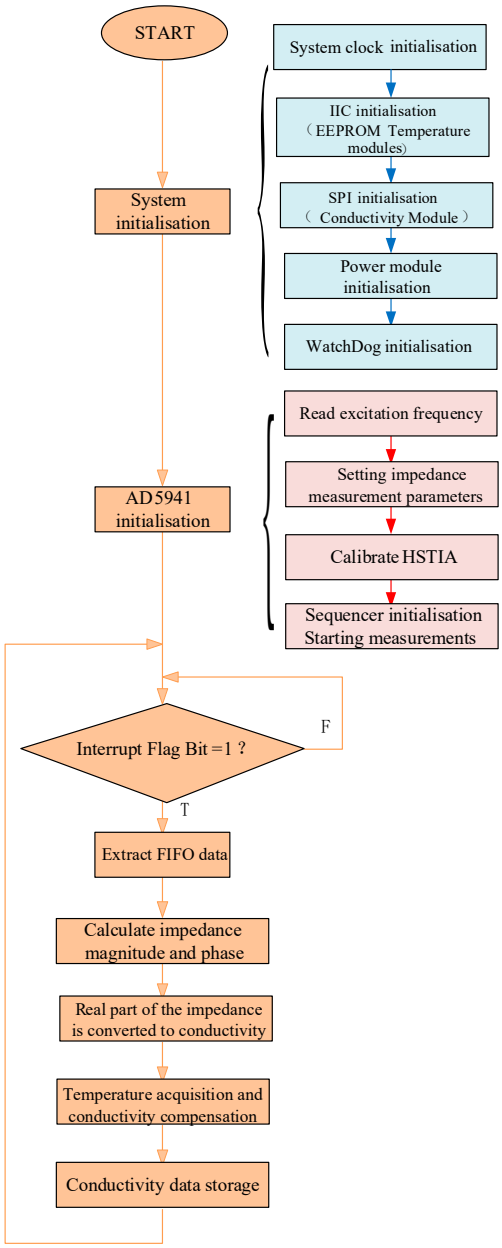

Figure 6. Flow chart of soil electrical conductivity detection software.

The primary function of the prototype's main program is to facilitate the acquisition, processing, and storage of soil electrical conductivity and soil temperature data. Utilizing the Software Development Kit (SDK, ad5940-examples v0.2.1) provided by Analog Devices Inc. (ADI, USA), the control program for the AD5941 chip is developed. This includes configuring registers, the programmable switch matrix, the programmable AFE sequencer, and other resources of the AD5941 chip. Additionally, algorithms for impedance calculation, soil electrical conductivity conversion, and temperature compensation are implemented to ensure accurate data processing and analysis.

2.3. Methods for Testing the Performance of Soil Electrical Conductivity Prototype

The performance of the soil electrical conductivity prototype is evaluated based on its calibration, encompassing both static and dynamic performance analyses. In this paper, the methodologies are primarily presented for testing various performance indices of the soil electrical conductivity prototype, including stability, steady−state error, response time, radial measurement range, and additional performance metrics.

2.3.1. Calibration Methods for Prototype

The calibration test of the soil electrical conductivity prototype was conducted using conductivity calibration solutions produced by Shanghai Leimagnet Instrument Co. At a room temperature of 25 °C, four calibration solutions with conductivities of 84 μS/cm, 146.5 μS/cm, 1408 μS/cm, and 12.85 mS/cm were contained in 100 mL tall beakers. The prototype probe was fully submerged in each solution, and the output was allowed to stabilize before readings were taken. This process was repeated ten times for each solution, with the average value recorded. After each calibration, the probe was cleaned with anhydrous ethanol and air−dried before proceeding to the next calibration to prevent contamination of the standard solutions and ensure measurement accuracy. The real part of the impedance (R) of the prototype output and the conductivity of the calibration solution (ECa) were determined, and the fitting function is depicted in Figure 7.

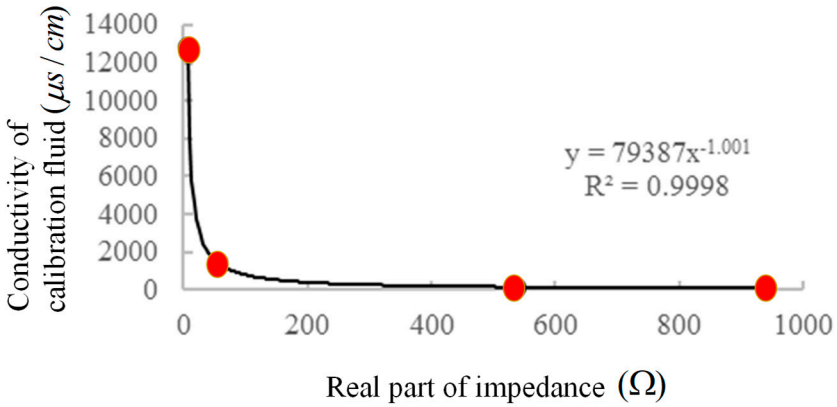

Figure 7. Calibration curve of soil electrical conductivity.

The relationship between soil electrical conductivity and real part of the impedance is as follows:

$$EC_a = 79,387R^{-1.001} \quad (5)$$

The coefficient of determination R^2 of EC_a is 0.9998, which corroborates that the conductivity of Equation (3) is the reciprocal of the real part of the impedance, with a constant coefficient corresponding to 79,387, which is written into the EEPROM of the prototype to complete the calibration of the conductivity.

2.3.2. Static Performance Analysis and Dynamic Performance Test Methods for Prototype

Soil samples with specific conductivity values were prepared to obtain measurement data from the soil electrical conductivity prototype at a room temperature of 25 °C. Each measurement was repeated 60 times. Through mathematical statistics, the relative standard deviation of the test data was calculated to analyze the prototype's stability. Both the standard deviation and the relative standard deviation were computed to verify the stability of the prototype. Additionally, the steady−state error was calculated to assess the detection accuracy of the prototype.

At a room temperature of 25 °C, soil samples with specific conductivity values were prepared. The self−made soil electrical conductivity probe was swiftly inserted from the air into the samples. The real part of the measured impedance was converted to soil electrical conductivity using the calibration function. The time required for the measured value to reach a stable range was recorded as the response time of the prototype.

2.3.3. Prototype Measurement Radial Sensitivity Range Test Methods

A soil sample with a specific conductivity value was prepared and packed into a Plexiglas cylinder with an inner diameter of 14 cm. The prototype was inserted into the soil sample from the center to measure the real value of the impedance output from

the conductivity module. Due to the probe's diameter of 1.6 cm, repeated insertions for measurement can damage the surrounding soil, causing improper contact between the metal ring and the soil. Therefore, maintaining the probe's insertion position, the Plexiglas cylinder was carefully removed along the prototype cable. Using a spatula, the soil sample was reduced by 0.5 cm to 0.7 cm in thickness, and the residual soil was packed into a Plexiglas cylinder with an inner diameter of 12 cm for further measurement. This process was repeated, reducing the inner diameter of the cylinder to 14 cm, 12 cm, 10 cm, 8 cm, 6 cm, and finally 4 cm (as shown in Figure 8). The prototype's output was recorded at each step until it stabilized, indicating the prototype's radial sensitivity range.

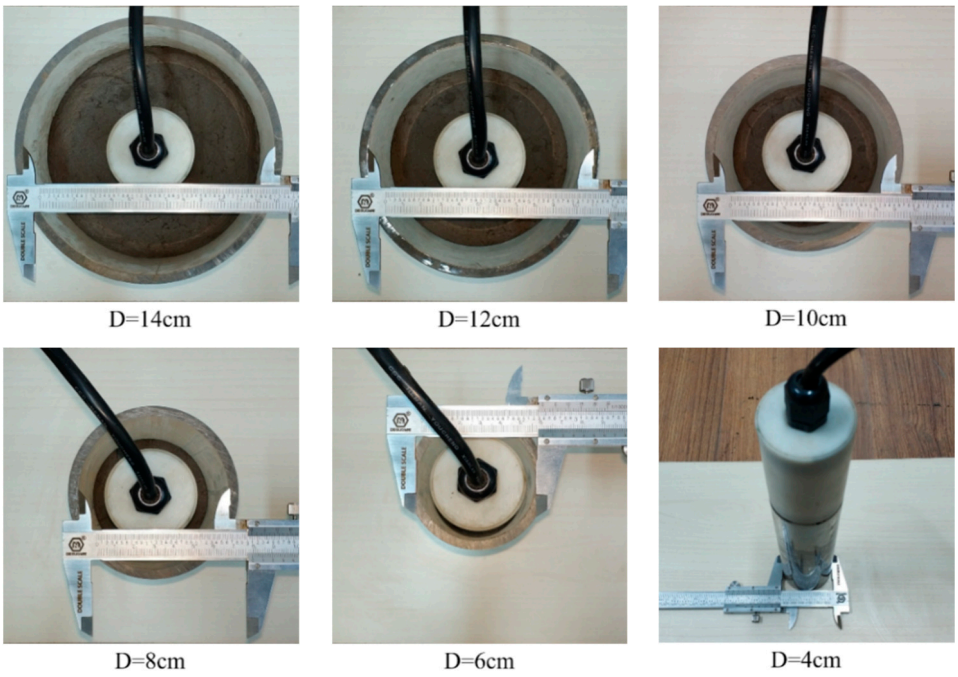

Figure 8. Soil electrical conductivity prototype's radial sensitivity range test procedure.

2.4. Soil Electrical Conductivity Temperature Compensation Algorithm

Soil dielectric properties are significantly affected by temperature [26,27], which leads to increased measurement errors. In this paper, the soil electrical conductivity was calibrated to the calibrated value of 25 °C by a temperature compensation algorithm to reduce the measurement error of the prototype.

From previous studies, it is known that the relationship between soil electrical conductivity and temperature can be expressed by the following equation [28,29]:

$$\sigma = \sigma_0 \left[1 + k_1(T - T_0) + k_2\left(T - T_2\right)^2\right] \tag{6}$$

where σ and σ_0 denote the conductivity at temperatures T and T_0, K_1, and K_2 denote the temperature compensation coefficients. Usually, since the effect of the quadratic term is small and can be neglected, Equation (6) simplifies to the following:

$$\sigma = \sigma_0[1 + k_1(T - T_0)] \tag{7}$$

In order to facilitate comparisons between different sensors and to take into account the environment in which the sensors are used, the temperature at which conductivity values are compensated is usually set at 25 °C.

3. Results

3.1. Prototype Structure Analysis

The diameter, width, and intervals of the four stainless steel rings in the four−ring probe significantly influence the measurement output of the conductivity sensor. To determine the optimal combination of these dimensions, 16 ring probes with varying specifications were prepared, encompassing four sizes for each of the three parameters. A three−factor, four−level orthogonal test was designed and conducted [30]. Measurements were performed in a conductivity standard solution of 545 µS/cm [31]. The parameters of the probes and the experimental results are detailed in Table 1, with the excitation frequency of the conductivity probe set at 100 kHz.

Table 1. Orthogonal test table for ring probes of different sizes.

Diameter (mm)	Width (mm)	Intervals (mm)	Impedance Amplitude (Ohm, 100 kHz)
16	4	4	112.74
16	**6**	**6**	**119.20**
16	8	8	131.24
16	10	10	151.68
18	4	6	107.46
18	6	4	103.02
18	8	10	142.23
18	10	8	136.54
20	4	8	104.57
20	6	10	127.16
20	8	4	99.78
20	10	6	115.06
22	4	10	111.47
22	6	8	108.65
22	8	6	104.37
22	10	4	98.34

The orthogonal test data were analyzed using SPSS software (SPSS 17.0). The results obtained are shown in Table 2:

Table 2. SPSS analysis of orthogonal test of ring probe.

Parameters	Type III ANOVAs	Degrees of Freedom	Mean Square	F	Statistical Significance
Correction model	3804.917 [a]	9	422.769	26.910	0.000
Intercept	219,377.483	1	219,377.483	13,963.721	0.000
Diameter (mm)	**1286.606**	**3**	**428.869**	**27.298**	**0.001**
Width (mm)	**582.594**	**3**	**194.198**	**12.361**	**0.006**
Intervals (mm)	**1935.716**	**3**	**645.239**	**41.070**	**0.000**
Inaccuracy	94.263	6	15.711		
Total	223,276.663	16			
Revised total	3899.180	15			

[a] R^2 = 0.976 (after adjusting R^2 = 0.940).

The analysis results indicate that the p−values associated with the three geometrical parameters of the probe are as follows: diameter (0.001), width (0.006), and spacing (0.000). The order of influence on the conductivity prototype's output, from most to least significant, is spacing, diameter, and width. The measured impedance amplitude is directly proportional to the ring's interval and width and inversely proportional to the ring's diameter. Considering the measurement accuracy, prototype practicality, and minimal disturbance to the surrounding soil, the optimal dimensions for the prototype 's ring probe are set to a

diameter of 16 mm, a width of 6 mm for the stainless−steel electrodes, and an electrode spacing of 6 mm.

3.2. Performance Testing and Analysis of Soil Electrical Conductivity Prototype

3.2.1. Static Performance Testing and Analysis of Soil Electrical Conductivity Prototype

The specific steps of the stability test are as follows:

(1) The soil was obtained from the teaching experimental forest farm of Beijing Forestry University in Sujiatuo Township, northwestern Haidian District, Beijing, where the soil type was clay loam [32]. Soil samples with a conductivity of 2250 μS/cm (measured using a Spectrum model 2265FS portable (Spectrum Technologies, Inc. USA) [33] soil electrical conductivity meter) were prepared by taking 2 kg of dried soil at a room temperature of 25 °C and sealing them in a large beaker to rest for 12 h;
(2) The rested samples were then placed in a thermostat set at 25 °C for 1 h;
(3) The prototype was inserted into the soil sample, and after allowing the readings to stabilize, data were collected every 2 min over a period of 2 h, resulting in a total of 60 measurements. The data obtained during the 2− h period were analyzed, as shown in Table 3 and Figure 9.

Table 3. Error analysis of the soil electrical conductivity prototype.

Parameter	Conductivity
mean value	2257.9072 μS/cm
standard deviation	1.2934 μS/cm
relative standard deviation	0.0573%
steady−state errors	<±2%

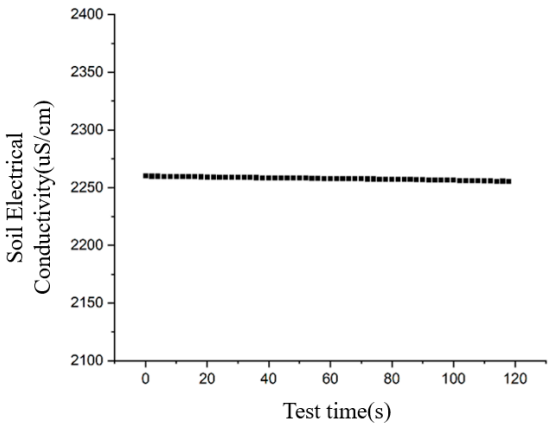

Figure 9. Soil electrical conductivity prototype's stability test.

The relative standard deviations of the test data are all as low as 0.0573%, indicating no significant variations within the dataset. This demonstrates that the prototype designed in this study exhibits excellent stability. Moreover, the steady−state error is minimal, making the prototype suitable for in situ measurements.

3.2.2. Dynamic Performance Testing and Analysis of Soil Electrical Conductivity Prototype

Soil samples with a water content of 15% and a conductivity of 430 μS/cm (measured using a Spectrum model 2265FS portable soil electrical conductivity meter) were prepared at a room temperature of 25 °C. The probe was swiftly inserted into the soil, and the real part of the measured impedance was converted to soil electrical conductivity using the calibration function of Equation (5) shown in Figure 10. In Figure 10, the horizontal axis represents the seconds from the timestamp of each data point, while the vertical axis represents the converted soil electrical conductivity. It is evident that the conductivity

module completes each impedance measurement within 50 ms, and the time required for the readings to stabilize is within 330 ms.

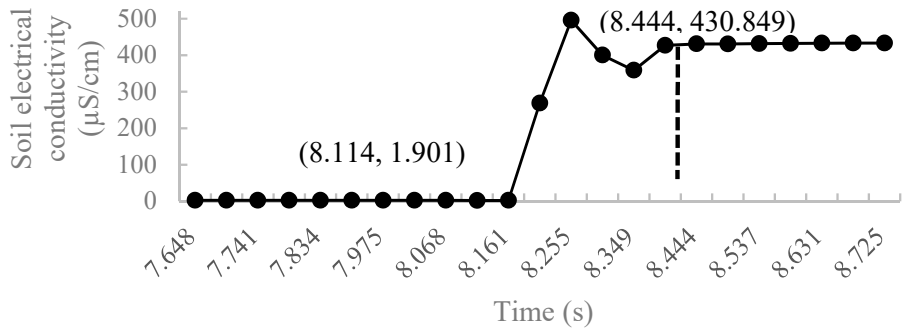

Figure 10. Dynamic response curve of soil electrical conductivity prototype.

3.2.3. Testing and Analyzing the Radial Sensitivity Range of Prototype Measurements

Soil samples with a conductivity of 792 μS/cm were prepared, and the measurement diameter was varied to obtain the following prototype outputs for six different gradients: 14 cm, 12 cm, 10 cm, 8 cm, 6 cm, and 4 cm. The results are depicted in Figure 11, which shows the conductivity values measured by the prototype for different diameters. As illustrated in Figure 11, the prototype's measured conductivity increases with the diameter of the soil samples. Beyond a diameter of 10 cm, the conductivity readings stabilize. This indicates that the prototype's effective measurement sensitivity is within a diameter of 10 cm.

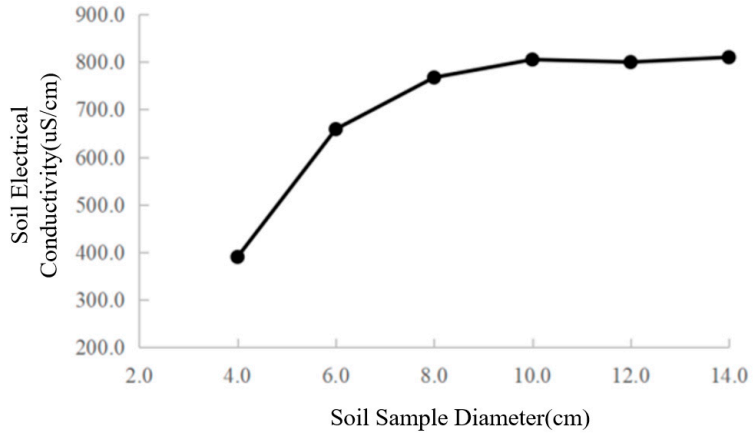

Figure 11. Experiment results of the radial sensitivity range of the soil electrical conductivity prototype.

3.2.4. Comparative Performance Tests

To assess the potential of the prototype as a replacement for commercially available foreign products, comparative performance tests were conducted. Six soil samples with varying conductivity gradients were prepared. The widely recognized 2265FS portable soil electrical conductivity meter, produced by Spectrum, was selected as the benchmark instrument. This meter features the following three measurement ranges: 0.0–200.0 μS/cm, 200–2000 μS/cm, and 2.00–20.00 mS/cm, with corresponding resolutions of 0.1 μS/cm, 1 μS/cm, and 0.01 mS/cm. Its measurement accuracy is 1.0% of the full−scale range for the selected gear. The conductivity of the six soil samples was measured using both the prototype and the Spectrum 2265FS meter at 25 °C. The comparative test results are presented in Figure 12.

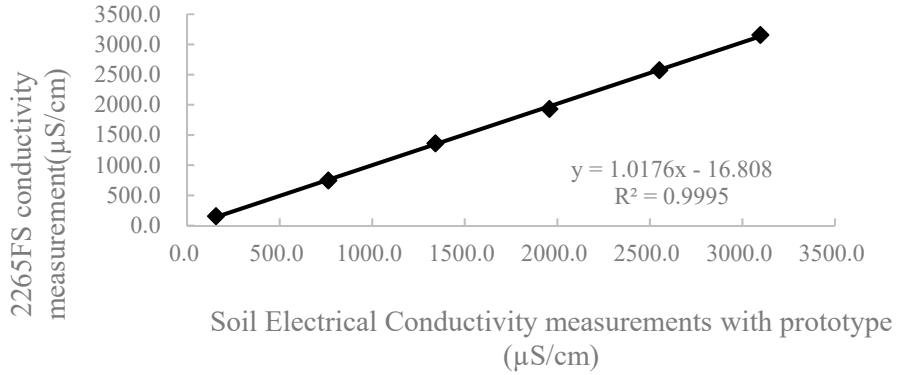

Figure 12. Soil electrical conductivity comparison test results.

The specific data, error ranges and prices of the comparison tests are shown in Tables 4 and 5.

Table 4. Comparison of soil electrical conductivity measurement between 2265FS sensor and the prototype.

Salinity (%)	0.00	0.05	0.10	0.15	0.20	0.25
2265FS measured value (μS/cm)	157.30	748.20	1363.30	1932.50	2575.90	3157.60
Measured values of prototype (μS/cm)	155.60	762.10	1341.20	1956.40	2551.00	3096.20
Absolute error (μS/cm)	1.70	13.90	22.10	23.90	24.90	61.40
Relative error (%)	1.08	1.86	1.62	1.24	0.97	1.94

Table 5. Comparison of main parameters between 2265FS sensor and the prototype.

	Soil Electrical Conductivity Prototype	Spectrum 2265FS	FOM2/mts
Electricity	5 V~12 V DC	6 V DC	3.7 V DC
Soil electrical conductivity measurement range	0.00~15.00 mS/cm	0.00~19.99 mS/cm	0.00~10.00 ms/cm
Soil electrical conductivity measurement accuracy	±2% FS	±1% FS	±10% FS
Prices	1500 CNY	4500 CNY	>10,000 CNY

As illustrated in Figure 12, the linear fitting curve for the measurements obtained from both the prototype and the 2265FS sensor is (y = 1.10176x − 16.808), with a coefficient of determination (R^2) of 0.9995. The absolute error ranges from −61.40 μS/cm to 23.90 μS/cm, while the relative error ranges from −1.94% to 1.86%. These results demonstrate that the accuracy of the prototype is comparable to that of the 2265FS sensor, indicating that its performance is effectively on par with the commercial standard.

3.3. Analysis of Conductivity Temperature Compensation

The test results were processed using the compensation function described in Equation (7), and the resulting temperature compensation coefficients were averaged to yield (k = 0.0198). Post−compensation, the absolute errors ranged from −93.35 μS/cm to 92.57 μS/cm, and the relative errors ranged from −2.72% to 2.87%. Figure 13 illustrates the comparison of two soil sample groups with conductivities of 805.1 μS/cm and 3814.8 μS/cm

before and after temperature compensation, showing a significant reduction in measurement error.

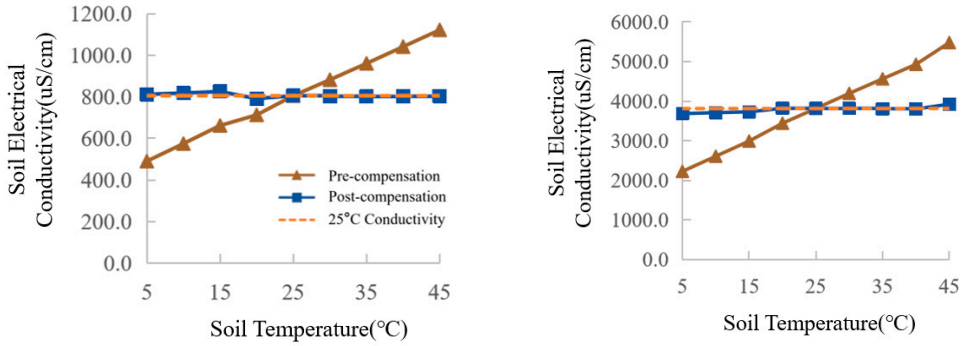

Figure 13. Comparison of prototype's soil electrical conductivity temperature compensation effect. (**a**) The electrical conductivity of the soil sample was 805.1 μScm. (**b**) The electrical conductivity of the soil sample was 3814.8 μS/cm.

4. Discussion

The results of this study highlight the potential of reducing the cost of soil electrical conductivity detection and reducing the effect of temperature on the accuracy of soil electrical conductivity measurements, thereby increasing its potential to be widely used. In this paper, the feasibility of a in situ online soil electrical conductivity detection prototype is proposed and validated, based on the AD5941 for the limitations of the classical four−terminal method soil electrical conductivity detection principle with a constant current source, and the detection accuracy is improved by temperature compensation. The results of the comparative study with the commercial sensor (2265FS portable soil electrical conductivity meter) show that the measurement accuracy of both are similar, and the linear fit, absolute error range, and relative error range are similar. This indicates that the performance of the prototype has been comparable to that of the commercialized sensor, but the price is much lower than that of the commercialized sensor.

In the structural design, the focus in this study was on solving the problem of inconvenience and easy damage of traditional multi−pin sensors, and a cone−type probe was used to make the prototype more stable. In the hardware design, the low−power analogue front−end chip AD5941 was selected to achieve the absolute impedance measurement of the four−terminal method, so as to achieve the purpose of measuring soil electrical conductivity and effectively reduce the cost of the prototype.

Although in this study the performance test of the original soil conductivity detection machine was carried out with a clay loam soil from the teaching experimental forestry farm of Beijing Forestry University in Sujiatuo Township, northwestern Haidian District, Beijing, as a sample and a series of research results were obtained, it is necessary to add more types of soils as the research samples in order to further advance the depth of this study, for example, sandy soils, clay soils, and so on. We can build a soil electrical conductivity calibration model based on soil type criteria to better facilitate usage.

5. Conclusions

This study aimed to improve the current real−time soil electrical conductivity detection device in its practical application and in view of it being highly affected by temperature, inconvenient to use, expensive, and other issues. The main contributions are as follows:

(1) The AD5941 chip was chosen to improve the four−terminal method soil electrical conductivity measurement principle, eliminating the dependence on the constant current source, optimizing the design of the soil electrical conductivity detection hardware circuit, and improving the integration degree of the prototype by using its internal DDS, ADC, and DFT modules;

(2) The American Society of Agricultural Engineers (ASAE) standards were followed, the conical probe structure of the four−ring metal electrode was optimized, and a new conical probe was designed. The orthogonal test was conducted to verify the reasonableness of its mechanical structure for the measurement of soil electrical conductivity, and to improve the convenience of use;
(3) The detection accuracy of the prototype was improved by the temperature compensation algorithm;
(4) The relevant test results showed that the relative error of measurement of the soil electrical conductivity prototype was within ±2%; the relative standard deviation of the test data was 0.0573%, and there were no obvious differences in the data within the group; the dynamic response time was less than 50 ms; and the radial sensitivity range was 8~10 cm;
(5) The results of the comparative study between the prototype and the commercialized sensor showed that the linear fit of the two measurements reaches 0.9995, with an absolute error range of −61.40 μS/cm~23.90 μS/cm, and a relative error range of −1.94%~1.86%. The prototype in this paper was comparable to the performance of marketed products in terms of performance indicators, and also significantly reduced the cost.

Author Contributions: Conceptualization, R.S.; methodology, R.S.; software, R.S.; validation, R.S.; formal analysis, R.S.; investigation, R.S.; data curation, R.S.; writing—original draft preparation, R.S.; writing—review and editing, M.Z. and R.S; supervision, M.Z. All authors have read and agreed to the published version of the manuscript.

Funding: This research received no external funding.

Institutional Review Board Statement: Not applicable.

Informed Consent Statement: Not applicable.

Data Availability Statement: The original contributions presented in this study are included in the article; further inquiries can be directed to the corresponding authors.

Conflicts of Interest: The authors declare no conflict of interest.

References

1. Othaman, N.N.; Isa, M.N.; Ismail, R.C.; Ahmad, M.I.; Hui, C.K. Factors that affect soil electrical conductivity (EC) based system for smart farming application. In Proceedings of the AIP Conference Proceedings, Putrajaya, Malaysia, 8 January 2020.
2. Pan, Z.L.; Liu, H.F.; Zhao, S.X. Effects of Nutrient Supply Based on Soil EC Control on Tomato Growth, Yield and Quality. *Soil Fertil. Sci. China* **2022**, *1*, 163–171.
3. Cao, Y.; Huang, H.Y.; Wu, H.S.; Xu, Y.D.; Chen, Y.J. Mechanisms of ultrahigh-temperature composting to improve soil nutrient effectiveness and rice yield. *J. Plant Nutr. Fertil.* **2020**, *26*, 481–491.
4. Robinet, J.; von Hebel, C.; Govers, G.; van der Kruk, J.; Minella, J.P.; Schlesner, A.; Ameijeiras−Mariño, Y.; Vanderborght, J. Spatial Variability of Soil Water Content and Soil Electrical Conductivity Across Scales Derived from Electromagnetic Induction and Time Domain Reflectometry. *Geoderma* **2018**, *314*, 160–174. [CrossRef]
5. Lu, C.; Lu, J.; Zhang, Y.; Puckett, M.H. A Convenient Method to Estimate Soil Hydraulic Conductivity Using Electrical Conductivity and Soil Compaction Degree. *J. Hydrol.* **2019**, *575*, 211–220. [CrossRef]
6. Deng, X.; Gu, H.; Yang, L.; Lyu, H.; Cheng, Y.; Pan, L.; Fu, Z.; Cui, L.; Zhang, L. A Method of Electrical Conductivity Compensation in a Low−cost Soil Moisture Sensing Measurement Based on Capacitance. *Measurement* **2020**, *150*, 107052. [CrossRef]
7. Rhoades, J.D.; van Schilfgaarde, J. An Electrical Conductivity Probe for Determining Soil Salinity. *Soil Sci. Soc. Am. J.* **1976**, *40*, 647–651. [CrossRef]
8. De Jong, E.; Ballantyne, A.K.; Cameron, D.R.; Read, D. Measurement of Apparent Electrical Conductivity of Soils by an Electromagnetic Induction Probe to Aid Salinity Surveys. *Soil Sci. Soc. Am. J.* **1979**, *43*, 810–812. [CrossRef]
9. Zhang, Q.; Fu, Y. Portable Soil Electrical Conductivity Sensor System Based on Electromagnetic Pulsed Eddy Current Method. In *Proceedings of IOP Conference Series: Earth and Environmental Science, 2020*; IOP Publishing: Bristol, England, 2020.
10. Tsuchikawa, S.; Ma, T.; Inagaki, T. Application of Near−infrared Spectroscopy to Agriculture and Forestry. *Anal. Sci.* **2022**, *38*, 635–642. [CrossRef] [PubMed]
11. Pei, X.; Sudduth, K.A.; Veum, K.S.; Li, M. Improving In−situ Estimation of Soil Profile Properties Using a Multi−sensor Probe. *Sensors* **2019**, *19*, 1011. [CrossRef]

12. Yandong, Z.; Ning, L.; Tingling, P. Soil Electrical Conductivity Online Real−time Detection System Based on Four−electrode Method. *Trans. Chin. Soc. Agric. Mach.* **2015**, *46*, 299–307.
13. Pei, X.; Meng, C.; Li, M.; Yang, W.; Zhou, P. Measurement of Soil Electrical Conductivity Based on Direct Digital Synthesizer (DDS) and Digital Oscilloscope. *Int. J. Agric. Biol. Eng.* **2019**, *12*, 162–168. [CrossRef]
14. Zhong, X.; Yang, L.; Zhang, D.; Cui, T.; He, X.; Du, Z. Design and Experiment of a Sensor for In−situ Rapid Detection of Soil Electrical Conductivity Using Four−electrode Method. *Trans. Chin. Soc. Agric. Eng. (Trans. CSAE)* **2021**, *37*, 90–99.
15. Yang, W.; Han, Y.; Li, M.; Meng, C. Vehicle Mounted Soil Electrical Conductivity Detection System Based on Digital Oscilloscope. *Trans. Chin. Soc. Agric. Mach.* **2020**, *51*, 395–401.
16. Rusu, C.; Krozer, A.; Johansson, C.; Ahrentorp, F.; Pettersson, T.; Jonasson, C.; Rösevall, J.; Ilver, D.; Terzaghi, M.; Chiatante, D. Miniaturized Wireless Water Content and Conductivity Soil Sensor System. *Comput. Electron. Agric.* **2019**, *167*, 105076. [CrossRef]
17. Pei, X.; Sun, H.; Zheng, L.; Li, M. Development of Movable Acquisition System for Soil Optical−electrical Parameters. *Nongye Jixie Xuebao/Trans. Chin. Soc. Agric. Mach.* **2015**, *46*, 90–95.
18. Mu, W.; Han, N.; Qu, Z.; Zheng, M.; Shan, Y.; Guo, X.; Sun, Y.; Mu, Y. ECWS: Soil Salinity Measurement Method Based on Electrical Conductivity and Moisture Content. *Agronomy* **2024**, *14*, 1345. [CrossRef]
19. Han, Y.; Yang, W.; Li, M.; Meng, C. Comparative Study of Two Soil Electrical Conductivity Meters Based on the Principle of Current−voltage Four−terminal Method. *IFAC Pap.* **2019**, *52*, 36–42.
20. Murata, H.; Futagawa, M.; Kumazaki, T.; Saigusa, M.; Ishida, M.; Sawada, K. Millimeter Scale Sensor Array System for Measuring the Electrical Conductivity Distribution in Soil. *Comput. Electron. Agric.* **2014**, *102*, 43–50. [CrossRef]
21. Rhoades, J.D. Soil Electrical Conductivity and Soil Salinity: New Formulations and Calibrations. *Soil Sci. Soc. Am. J.* **1976**, *40*, 651–655. [CrossRef]
22. Sun, Y.; Lammers, P.S.; Damerow, L. A Dual Sensor for Simultaneous Investigation of Soil Cone Index and Moisture Content. *Agrartech. Forsch.* **2003**, *9*, E12–E16.
23. Hansen, B.; Schjønning, P.; Sibbesen, E. Roughness Indices for Estimation of Depression Storage Capacity of Tilled Soil Surfaces. *Soil Tillage Res.* **1999**, *52*, 103–111. [CrossRef]
24. Whalley, W.R.; Stafford, J.V. Real−time Sensing of Soil Water Content from Mobile Machinery: Options for Sensor Design. *Comput. Electron. Agric.* **1992**, *7*, 269–284. [CrossRef]
25. Wu, J.; Bai, W.; Zhang, L.; Zhang, X.; Lin, H.; Dai, H.; Liu, J.; Zhang, F.; Yang, Y. Design of a Portable Electrochemical Impedance Spectroscopy Measurement System Based on AD5941 for Lithium−ion Batteries. *J. Energy Storage* **2024**, *84*, 110856. [CrossRef]
26. Zhao, Y.; Chen, Z.; Gao, Z.; Zhang, X.; Yu, F. Temperature Drift Characteristics and Compensation of SWR Soil Moisture Sensor. *Trans. Chin. Soc. Agric. Mach.* **2019**, *50*, 257–263.
27. Or, D.; Wraith, J.M. Temperature Effects on Soil Bulk Dielectric Permittivity Measured by Time Domain Reflectometry: A Physical Model. *Water Resour. Res.* **1999**, *35*, 371–383. [CrossRef]
28. Asgari, M.; Lee, K. Fully−integrated CMOS Electrical Conductivity Sensor for Wet Media. *IEEE Sens. J.* **2019**, *19*, 6445–6451. [CrossRef]
29. Wild, J.; Kopecký, M.; Macek, M.; Šanda, M.; Jankovec, J.; Haase, T. Climate at Ecologically Relevant Scales: A New Temperature and Soil Moisture Logger for Long−term Microclimate Measurement. *Agric. For. Meteorol.* **2019**, *268*, 40–47. [CrossRef]
30. Zhang, X.; Liu, M.; Zhou, Y. Orthogonal Uniform Composite Designs. *J. Stat. Plan. Infer.* **2020**, *206*, 100–110. [CrossRef]
31. Li, C.; Lu, Y.; Chi, Y.; Chiu, C.; Lin, T. Dielectric Constant Measurement System Based on Rapid Switching. In Proceedings of the Asia−Pacific Microwave Conference (APMC), Taipei, Taiwan, 5 December 2023; IEEE: Boca Raton, FL, USA, 2023.
32. Zhou, J.M.; Shen, R.F. *Dictionary of Soil Science*; Science Press: Beijing, China, 2013.
33. Spectrum Technologies, Inc. Direct Soil EC Meter Product Manual [EB/OL]. Available online: www.manualslib.com/manual/1279834/Spectrum%E2%88%92Fieldscout%E2%88%922265fs.html?page=1#manual (accessed on 17 March 2024).